

High- Q Fully Reconfigurable Tunable Bandpass Filters

Himanshu Joshi, *Student Member, IEEE*, Hjalti H. Sigmarsson, *Student Member, IEEE*, Sungwook Moon, *Student Member, IEEE*, Dimitrios Peroulis, *Member, IEEE*, and William J. Chappell, *Member, IEEE*

Abstract—In this paper, the authors present a design technique that enables inter-resonator and external coupling control for high-quality-factor (Q) tunable bandpass filters. The design incorporates low- Q varactors as part of the inter-resonator and external coupling mechanisms without degrading the overall high Q of the original filter. Detailed design methodology and equations are presented to illustrate the concepts. A first-time demonstration of these concepts is presented for a widely tunable high- Q evanescent-mode cavity bandpass filter. The cavities are integrated in a low-loss substrate with commercially available piezoelectric actuators and solid-state varactors for frequency and bandwidth tuning. This technique allows for reduced bandwidth variation over large tuning ranges. As one example, a constant 25-MHz absolute-bandwidth filter in the 0.8–1.43-GHz tuning range with loss that is as low as 1.6 dB is presented as an example. The filter third-order intercept point is between 32.8 and 35.9 dBm over this tuning range. To further show the impact of the technique on high- Q filters, a filter Q that is as high as 750 is demonstrated in the range of 3–5.6 GHz, while using low- Q varactors ($Q < 30$ at 5 GHz for a 0.4-pF capacitance) to achieve more than 50% reduction in bandwidth variation over the tuning range.

Index Terms—Cavity resonators, evanescent-mode filters, piezoelectric transducers, tunable filters.

I. INTRODUCTION

NEXT-GENERATION wireless systems may require reconfigurable bandpass filters for front-end preselection to enable multiband operation [1]. A lot of research has been done on the center-frequency adaptable bandpass filters, and they have been realized in different technologies, notably microelectromechanical systems (MEMS) [2], [3], ferroelectric thin films [4], and evanescent-mode cavity filters [5]–[7]. For a reconfigurable filter, it is essential to have control over not only the center frequency but also the bandwidth of the filter. This is because the filter bandwidth is proportional to the center frequency [8] and can therefore vary significantly over wide tuning ranges. This bandwidth variation can significantly be reduced for a varactor-tuned combline filter topology by appropriately designing the transmission lines in the resonator [9], [10]. By

using independent electric and magnetic field coupling, predefined bandwidth characteristics have also been demonstrated for the same electrical length of the resonators [11]. To achieve dynamic control over the bandwidth as a function of the filter center frequency, tunable components have also been incorporated in the inter-resonator coupling mechanism in the form of varactor diodes [12], [13] or MEMS cantilevers [14]. However, tunable components generally have much lower quality factors (Q) than tank resonators and can significantly degrade the performance of a high- Q filter. In this paper, the authors present an alternative approach for high- Q narrowband filters, where the low- Q tunable components such as varactors can be utilized for bandwidth control without significantly impacting the insertion loss.

For narrowband filters, the bandwidth can be changed significantly with only a small change in the inter-resonator coupling, and, therefore, the low- Q varactors do not have to be the dominant inter-resonator coupling mechanism. The varactors are incorporated in parallel with a low-loss inter-resonator coupling mechanism, which sets the initial bandwidth of the filter. To achieve a good impedance match to this bandwidth control design, a tunable external coupling design using low- Q varactors is also implemented which allows additional control over the shape/group delay of the filter. The tunable tank resonators for center frequency tuning are shielded from these low- Q varactors using transformers, which allow bandwidth and external coupling control while maintaining high Q of the filter. A first-time demonstration of these concepts for evanescent-mode cavity filters [15], [16] fabricated in a low-loss Rogers trimethylenemethane (TMM) substrate is presented.

In [17], the authors had presented inter-resonator coupling control for these filters, demonstrating bandwidth control of up to 33% while maintaining at least 71.4% of the original Q . The extracted filter Q was in the range of 250–350, even though low- Q varactors ($Q < 30$ at 1 GHz) with a capacitance in the 0.5–4-pF range were utilized in the inter-resonator coupling mechanism. A constant absolute-bandwidth 25-MHz tunable filter was also presented in the 0.89–1.47-GHz range, with less than 3 dB of insertion loss. However, these designs did not have tunable external coupling and, thus, did not allow full control over the filter group delay/out-of-band attenuation.

In this paper, the authors present an improved design additionally incorporating a tunable external coupling mechanism. The new design enables improved matching throughout the band, exemplified by a reduction in loss of up to 0.4 dB over the tuning range for the same 25-MHz bandwidth compared to the design in [17]. Additionally, the tunable external coupling

Manuscript received May 26, 2009; revised September 22, 2009. First published November 03, 2009; current version published December 09, 2009. This work was supported by the Defense Advanced Research Projects Agency Analog Spectral Processors Grant.

The authors are with the IDEAS Microwave Laboratory, Purdue University, West Lafayette, IN 47907 USA (e-mail: hjoshi@purdue.edu; hsigmars@purdue.edu; moon8@purdue.edu; dperouli@purdue.edu; chappell@purdue.edu).

Color versions of one or more of the figures in this paper are available online at <http://ieeexplore.ieee.org>.

Digital Object Identifier 10.1109/TMTT.2009.2034309

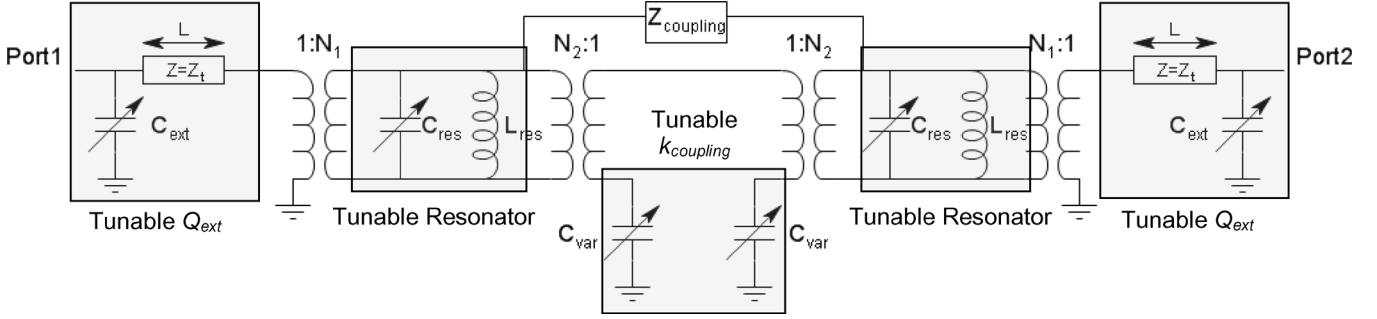


Fig. 1. Reconfigurable second-order filter schematic. All the tunable elements are emphasized by shaded boxes.

mechanism allows the control over the out-of-band attenuation/group delay of the filter which is also demonstrated. As a further demonstration, filter Q that is as high as 750 is demonstrated for filters in the 3–5.6-GHz range, while using varactors with Q less than 30 at 5 GHz. The bandwidth variation over the tuning range has been reduced by more than 50% compared to an inter-resonator coupling iris alone.

II. FILTER DESIGN

The reconfigurable filter schematic is shown in Fig. 1 and includes bandwidth and external coupling control in addition to center frequency tuning. For a high- Q filter, it is critical to achieve all these requirements without degrading the filter Q . This is particularly challenging since tunable lumped components are generally low Q and will hence reduce the overall filter Q . The filter schematic in Fig. 1 allows the possibility of using low- Q varactors to achieve bandwidth and external coupling control, without degrading the high Q of the filter. The filter consists of two high- Q tunable resonators modeled as equivalent lumped components, a tunable capacitor C_{res} and an inductance L_{res} at the center frequency (ω_0) of the filter. The impedance Z_{coupling} denotes the low-loss inter-resonator coupling between the two resonators and sets the initial bandwidth of the filter. For a narrow-bandwidth filter, $Z_{\text{coupling}} \gg \omega_0 L_{\text{res}}$ or $Z_{\text{coupling}} \gg 1/(\omega_0 C_{\text{res}})$ for inductive or capacitive coupling, respectively [18]. To tune the bandwidth, lumped varactors C_{var} are used in parallel with Z_{coupling} , connected to each resonator through transformers with a number of turns N_2 . The external coupling is controlled using the lumped varactors C_{ext} shielded from the high- Q resonator using a transformer at the input and output with number of turns N_1 . A transmission line with impedance Z_t and length L is used to control the external coupling variation over the tuning range. The major advantage of this design is that, for sufficiently large values of N_1 and N_2 , low- Q varactors C_{var} and C_{ext} can be used to control the shape of a narrowband high- Q filter, with little degradation in the overall Q of the filter.

The effect of C_{var} on the filter bandwidth can be understood by looking at the even and odd modes of the filter shown in Fig. 2(a) and (b), respectively. C_{var} only affects the odd mode of the filter and, therefore, can be used to change the bandwidth of the filter. The odd modes of the filter for an inductive (i.e., $Z_{\text{coupling}} = \omega_0 L_{\text{coupling}}$) and a capacitive coupling (i.e.,

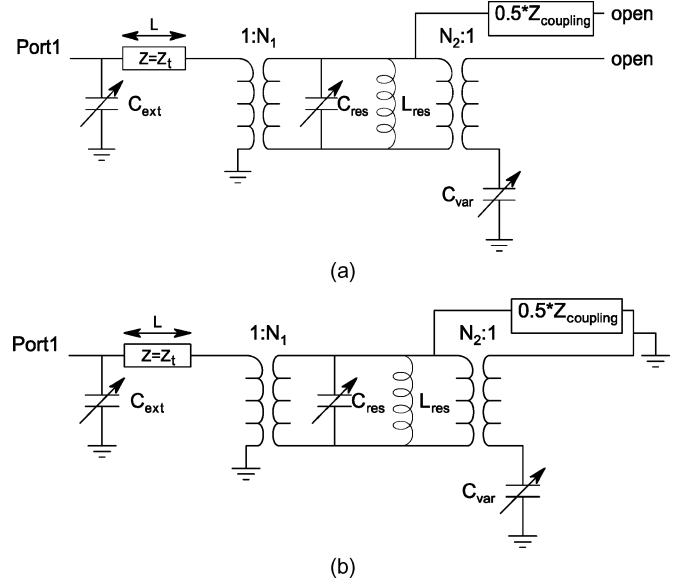


Fig. 2. Equivalent circuit schematic of the filter resonant modes. (a) Even mode. (b) Odd mode.

$Z_{\text{coupling}} = 1/(\omega_0 C_{\text{coupling}})$) network are described by (1) and (2) in the following, and the even mode is described by (3):

$$f_{\text{odd-cap}} = \frac{1}{2\pi} \frac{1}{\sqrt{(L_{\text{res}}) \left(C_{\text{res}} + \frac{C_{\text{var}}}{(N_2)^2} + 2C_{\text{coupling}} \right)}} \quad (1)$$

$$f_{\text{odd-ind}} = \frac{1}{2\pi} \frac{1}{\sqrt{\left(L_{\text{res}} \parallel \frac{L_{\text{coupling}}}{2} \right) \left(C_{\text{res}} + \frac{C_{\text{var}}}{(N_2)^2} \right)}} \quad (2)$$

$$f_{\text{even}} = \frac{1}{2\pi} \frac{1}{\sqrt{L_{\text{res}} C_{\text{res}}}}. \quad (3)$$

For large values of N_1 and N_2 and for a narrowband filter such that $(C_{\text{var}}/(N_2)^2) + 2C_{\text{coupling}} \ll C_{\text{res}}$ or $L_{\text{coupling}} \gg L_{\text{res}}$, (1) and (2) can be simplified to give

$$f_{\text{odd-cap}} \approx f_{\text{even}} \left(1 - \frac{C_{\text{var}}}{2(N_2)^2 C_{\text{res}}} - \frac{C_{\text{coupling}}}{C_{\text{res}}} \right) \quad (4)$$

$$f_{\text{odd-ind}} \approx f_{\text{even}} \left(1 + \frac{L_{\text{res}}}{L_{\text{coupling}}} - \frac{C_{\text{var}}}{2(N_2)^2 C_{\text{res}}} \right). \quad (5)$$

The percentage change in absolute bandwidth from the initial bandwidth due to the addition of C_{var} can be written as the

ratio of the change in the odd mode due to C_{var} to the original separation of the odd and even modes obtained using (3)–(5) as

$$\frac{f_{\text{odd_ind}} - f_{\text{odd_ind}}(C_{\text{var}} = 0)}{f_{\text{odd_ind}}(C_{\text{var}} = 0) - f_{\text{even}}} = \frac{-1}{2k_{\text{coupling_ind}}} \left(\frac{C_{\text{var}}}{(N_2)^2 C_{\text{res}}} \right) \quad (6)$$

$$\frac{f_{\text{odd_cap}} - f_{\text{odd_cap}}(C_{\text{var}} = 0)}{f_{\text{even}} - f_{\text{odd_cap}}(C_{\text{var}} = 0)} = \frac{1}{2k_{\text{coupling_cap}}} \left(\frac{C_{\text{var}}}{(N_2)^2 C_{\text{res}}} \right). \quad (7)$$

$k_{\text{coupling_cap}} = C_{\text{coupling}}/C_{\text{res}}$ and $k_{\text{coupling_ind}} = L_{\text{res}}/L_{\text{coupling}}$ are the coupling coefficients in the absence of C_{var} and are proportional to the filter fractional bandwidth for narrowband filters [18]. According to (6) and (7), the percentage change in bandwidth is inversely proportional to these coupling coefficients. This indicates that a narrower initial bandwidth, corresponding to a smaller coupling coefficient, would allow a larger percentage change for the same value of C_{var} . The addition of C_{var} changes the bandwidth from the initial bandwidth set by $k_{\text{coupling_ind}}$ or $k_{\text{coupling_cap}}$. The bandwidth decreases with increasing C_{var} for inductive coupling and increases for capacitive coupling, as seen from (6) and (7), respectively. The minimum desired percentage bandwidth change from the initial bandwidth, denoted by Δ_{min} , decides the minimum value of the varactor capacitance, obtained using (6) or (7) as

$$C_{\text{var}}(\text{min}) = 2\Delta_{\text{min}} k_{\text{coupling}} (N_2)^2 C_{\text{res}}. \quad (8)$$

The next step is to evaluate the effect of the varactor Q on the original filter Q , denoted by Q_{old} . It is estimated using the following equations:

$$Q_{\text{var}} = \omega_o R_{\text{var}} C_{\text{var}} \quad (9)$$

$$Q_{\text{old}} = \omega_o R_{\text{old}} C_{\text{res}} \quad (10)$$

$$Q_{\text{new}} \approx \omega_o (R_{\text{old}} \parallel (N_2)^2 R_{\text{var}}) C_{\text{res}} \quad (11)$$

where R_{var} is the shunt parasitic resistance of C_{var} and R_{old} is the shunt resistance in parallel with C_{res} . Equation (11) can be further simplified using (9) and (10) to give

$$Q_{\text{new}} \approx Q_{\text{old}} \left\| \frac{(N_2)^2 Q_{\text{var}} C_{\text{res}}}{C_{\text{var}}} \right. \quad (12)$$

The maximum value of the varactor capacitance is determined by the desired $Q_{\text{new}} = xQ_{\text{old}}$, where $0 < x < 1$, and can be obtained using (12) as

$$C_{\text{var}}(\text{max}) = \frac{(1-x)(N_2)^2 Q_{\text{var}} C_{\text{res}}}{xQ_{\text{old}}}. \quad (13)$$

In order for the design to be feasible, $C_{\text{var}}(\text{max})$ has to be greater than $C_{\text{var}}(\text{min})$ which places a limit on the largest coupling coefficient given by

$$k_{\text{coupling}}(\text{max}) = \frac{(1-x)Q_{\text{var}}}{2\Delta_{\text{min}} x Q_{\text{old}}}. \quad (14)$$

The coupling coefficient in (14) decides the initial bandwidth of the filter which is controlled using C_{var} .

Achieving external coupling control is important to enable impedance matching to this controllable bandwidth over large

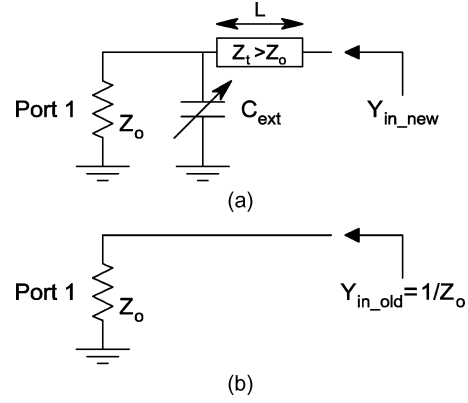


Fig. 3. Tunable Q_{ext} section. (a) With the external coupling network. (b) Without the external coupling network.

tuning ranges. The external Q for a bandpass filter is given by the following equation [18]:

$$Q_{\text{ext}} = \frac{g_0 g_1 f_o}{\text{BW}}. \quad (15)$$

From (15), the reduced bandwidth variation over a large tuning range requires an increased Q_{ext} , i.e., reduced external coupling at the high end of the tuning range, to allow good impedance matching. To achieve this, a short transmission line, shown in Figs. 1 and 3(a), of length $L < \lambda/4$ and impedance $Z_t > Z_o$ is used to tailor the external coupling as a function of the tuning range. In addition, the varactor C_{ext} is also used to achieve dynamic control over the external coupling. The effect of this external coupling section can be understood by comparing the real part of the admittance $Y_{\text{in_new}}$ and $Y_{\text{in_old}}$ as shown in Fig. 3(a) and (b). Q_{ext} can be related to the real part of the admittance using

$$Q_{\text{ext}} = \frac{(N_1)^2 \omega_o C_{\text{res}}}{\text{Re}(Y_{\text{in}})}. \quad (16)$$

For the same number of turns N_1 , the ratio of the new Q_{ext} with the external coupling section in Fig. 3(a) to the old Q_{ext} in Fig. 3(b) gives an indication of the change in external coupling and can be obtained using (16) as

$$\frac{Q_{\text{ext_new}}}{Q_{\text{ext_old}}} = \frac{\text{Re}(Y_{\text{in_old}})}{\text{Re}(Y_{\text{in_new}})}. \quad (17)$$

The new admittance can be calculated by approximating the short length of the transmission line as an inductor and is given by

$$Y_{\text{in_new}} = \frac{1}{\frac{Z_o}{1+j\omega Z_o C_{\text{ext}}} + jZ_t \beta L}. \quad (18)$$

The real and imaginary part of this admittance can be further obtained as

$$\text{Re}(Y_{\text{in_new}}) = \frac{Z_o}{(Z_o - Z_t \beta L \omega Z_o C_{\text{ext}})^2 + (Z_t \beta L)^2} \quad (19)$$

$$\text{Im}(Y_{\text{in_new}}) = \frac{\omega Z_o^2 C_{\text{ext}} - (\omega Z_o C_{\text{ext}})^2 Z_t \beta L - Z_t \beta L}{(Z_o - Z_t \beta L \omega Z_o C_{\text{ext}})^2 + (Z_t \beta L)^2}. \quad (20)$$

By substituting (19) into (17), the ratio of the new to old Q_{ext} can be estimated using the following equation:

$$\frac{Q_{\text{ext_new}}}{Q_{\text{ext_old}}} = (1 - Z_t \beta L \omega C_{\text{ext}})^2 + \left(\frac{Z_t \beta L}{Z_o} \right)^2. \quad (21)$$

The aforementioned expression indicates that Q_{ext} can be reduced by increasing the value of C_{ext} . To determine the effect of the transmission line by itself, consider the special case of $C_{\text{ext}} = 0$. For this case, (21) reduces to

$$\frac{Q_{\text{ext_new}}}{Q_{\text{ext_old}}} = 1 + \left(\frac{Z_t \beta L}{Z_o} \right)^2. \quad (22)$$

Q_{ext} can be therefore increased by using a short length of the high-impedance line. Furthermore, the external coupling will be reduced much more at the high end of the tuning range due to the linear dependence of β on ω . This will allow a good impedance match to the reduced bandwidth variation. While Q_{ext} can be reduced by just the transmission line, its variation as a function of frequency is predetermined. The addition of the varactor C_{ext} before the transmission line further allows dynamic control of the external coupling. From (21), Q_{ext} can be reduced by increasing the value of C_{ext} for fixed transmission line parameters. With this two-variable control (T-line and C_{ext}) of the external coupling, the filter response can be tailored to achieve the desired out-of-band attenuation/group delay over large tuning ranges. Another advantage of this design is that C_{ext} can be a low- Q varactor since the high- Q tank resonators are shielded from it by the input and output coupling transformers with N_1 number of turns.

These design concepts can be illustrated for a high- Q filter at 1.5 GHz with $C_{\text{res}} = 20$ pF. The original Q for such a filter without the addition of the low- Q varactors is chosen to be 500 and is referred to as Q_{old} . A coupling coefficient $k_{\text{coupling}} = 1.9\%$ is chosen which corresponds to a filter bandwidth of 40 MHz obtained using [18]. For a given Δ_{min} and $x = Q_{\text{new}}/Q_{\text{old}}$, the maximum coupling coefficient $k_{\text{coupling}(\text{max})}$ of the filter can be computed using (14). Furthermore, for a given k_{coupling} and N_2 , Δ_{min} and x can be estimated as a function of C_{var} using (8), (13), and (14). Fig. 4 shows the estimated change in Δ_{min} and x of the filter on increasing C_{var} ($Q_{\text{var}} = 20$ at 1.5 GHz) for $N_2 = 3$. From Fig. 4, increasing C_{var} up to 3.4 pF reduces the bandwidth from the initial value of 40 MHz by up to 50% ($\Delta_{\text{min}} = 0.5$), with the new Q being still 68% ($x = 0.68$) of the old Q . For $k_{\text{coupling}} = 1.9\%$ and $C_{\text{res}} = 20$ pF, L_{coupling} and L_{res} can be computed using the standard filter design equations in [18] as 29.7 and 0.57 nH, respectively.

To achieve good impedance matching to this tunable bandwidth, the tunable external coupling in Fig. 1 is implemented using the varactor C_{ext} modeled as a tunable capacitor with Q of 20 at 1.5 GHz and a maximum capacitance of 1 pF. The transmission line parameters are chosen to have an electrical length of 30° ($L = \lambda/12$) at 1.5 GHz and $Z_t = 100 \Omega$. Since a larger value of C_{ext} results in increased external coupling, as seen from (20), it should be reduced from 1 to 0.1 pF as the bandwidth is reduced on increasing C_{var} . The number of turns N_1 can be obtained by using (15), (16), and (19) for the initial bandwidth of 40 MHz when $C_{\text{var}} = 0$ and $C_{\text{ext}} = 1$ pF. For the case of a

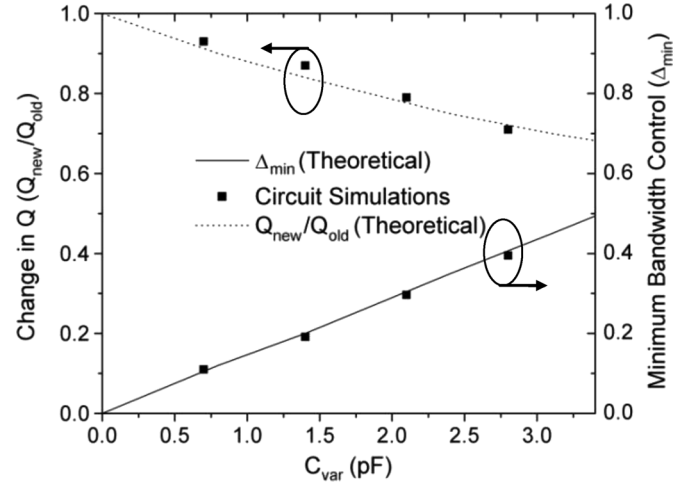


Fig. 4. Change in Q and bandwidth control as a function of C_{var} .

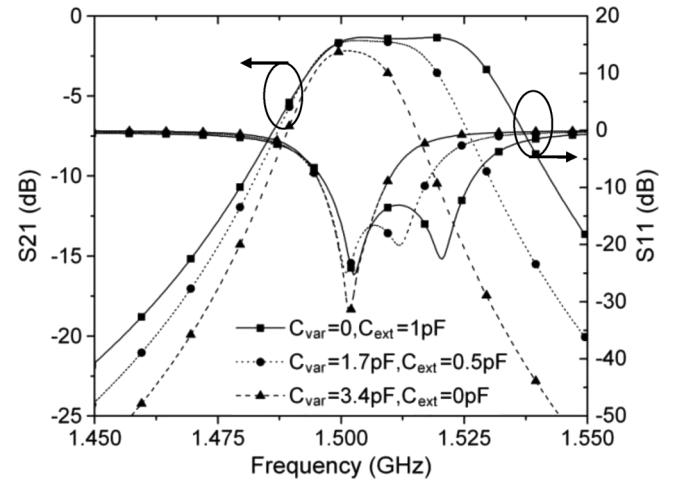


Fig. 5. Simulated results for the filter with bandwidth and external coupling control.

second-order maximally flat filter ($g_0 = 1, g_1 = 1.414$), a value of 2.5 is obtained for N_1 .

Since all the parameters in Fig. 1 are now determined, the filter response can be obtained using the Agilent Advanced Design System and is shown in Fig. 5. The bandwidth can be reduced from 40 to 21 MHz on increasing C_{var} from 0 to 3.4 pF, with the insertion loss being 1.3 and 2.3 dB, respectively. The value of C_{ext} is correspondingly reduced from 1 to 0 pF to maintain good impedance matching as the bandwidth is narrowed. The center frequency of the filter is slightly reduced since the bandwidth reduction only affects the odd-mode resonance. This can be compensated by tuning the tank resonators.

A comparison between the theoretical and simulated results is shown in Fig. 4 for four different values of C_{var} . There is a slight difference ($<5\%$) between the theoretical and simulated results due to the slight variation in the return loss in Fig. 5 as the filter bandwidth is narrowed. This is because the tunable input and output coupling networks also have a reactive component of the admittance given by (20) and are thus not ideal transformers. This reactive component, however, does not affect the location of the even- and odd-mode resonances as seen from Fig. 5. This

is because the shunt reactance from the tunable external coupling network being absorbed by the resonators is computed to be an effective inductance of 55.3 nH, which is significantly larger than the resonator inductance of 0.57 nH. The tunable external coupling network consisting of C_{ext} can be therefore used to achieve a good impedance match to a controllable bandwidth.

III. FILTER IMPLEMENTATION AND MEASUREMENT

In this section, the design concepts explained previously will be used to create high- Q evanescent-mode cavity filters [15], [16] with controllable bandwidths. By changing the capacitance created by the post in an evanescent-mode cavity filter, the filter can be tuned over wide frequency ranges [5]. By combining this wide-tuning and high- Q capability with inter-resonator and external coupling control, the response of the evanescent-mode cavity filter can be tailored to the desired specifications.

A. Constant Absolute-Bandwidth Design (0.8–1.43 GHz)

The layout of a high- Q evanescent-mode cavity filter design employing low- Q varactors for inter-resonator and external coupling control is shown in Fig. 6. The filter is designed using Ansoft HFSS in a 3.175-mm-thick Rogers TMM substrate with a dielectric constant of 3.2 and a loss tangent of 0.002. Conductive vias form the two resonators connected by a coupling iris as shown in Fig. 6(a). Each resonator has a capacitive post in the center created by four vias and a circular copper plate. The capacitive posts are on the top side of the substrate as shown in Fig. 6(a). A thin copper membrane is laminated on top of the substrate forming a gap between the post and top of the cavity, creating the tank capacitance C_{res} . A post radius of 3.5 mm is chosen, which corresponds to a resonator capacitance C_{res} of about 50 pF when the gap is 5 μm . The membrane is deflected using a commercially available 0.38-mm-thick piezoelectric disk actuator with a 12.7-mm diameter from Piezo Systems Inc. The actuator can provide up to 40 μm of free-free displacement.

The inter-resonator and external coupling control network is on the back side of the substrate as shown in Fig. 6(b). The bandwidth of the filter can vary significantly over large tuning ranges due to the frequency variation of the coupling iris. To control this bandwidth variation for achieving constant absolute bandwidth, the inter-resonator coupling control network consisting of the varactors C_{var} shown in Fig. 6(b) is used. Both the varactors are biased using the same voltage specified as V_{dc1} in Fig. 6(b). The slots in the bandwidth control network model act as transformers (N_2 turns) that connect the two resonators through the bandwidth control network. To use this bandwidth control for achieving reduced bandwidth variation over a large tuning range, the external coupling is also controlled using varactors corresponding to C_{ext} in Figs. 1 and 6(b). The input and output varactors are biased using independent voltages to control the filter shape/group delay. They are specified as V_{dc2} and V_{dc3} in Fig. 6(b). A high-impedance short length of line ($L = 5.3$ mm) of impedance $Z_t = 100 \Omega$ is used for controlling the variation of the external coupling over the tuning range.

Commercially available BB857 varactors from Infineon Technologies were used as C_{var} and C_{ext} to achieve inter-resonator and external coupling control, respectively. The var-

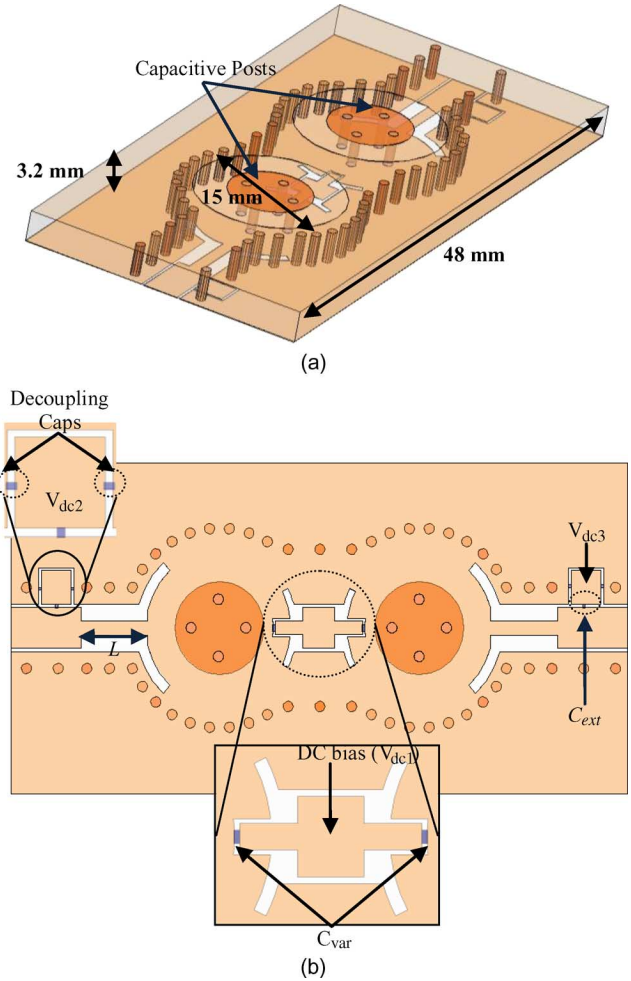


Fig. 6. Filter layout. (a) Top side having the capacitive posts. (b) Bottom side having the feed lines with the tunable bandwidth and external coupling section.

actors have a capacitance variation of 0.5–6.5 pF at 1 MHz on changing the reverse bias V_R from 28 to 1 V. The series resistance of the varactors is 1.5 Ω at 470 MHz for $V_R = 5$ V ($C_{\text{var}} \sim 2.5$ pF) [19], resulting in a Q of 60. Q_{var} can be therefore estimated to be 30 and 20 at 1 and 1.5 GHz, respectively, for a 2.5-pF capacitance.

The measured results are shown in Fig. 7 for a filter tuned from 0.8 to 1.43 GHz with constant 25-MHz absolute bandwidth. The estimated deflection of the copper membrane required for this tuning based on simulations is about 25 μm . The bandwidth of the filter is nearly constant at 25 MHz with a variation of only ± 0.27 MHz over the entire tuning range. The insertion loss is less than 3.1 dB over the entire tuning range, with a minimum of 1.6 dB in the range of 0.8–1 GHz. The estimated Q of the filter corresponding to this insertion loss variation is between 225 and 310 over the tuning range.

Fig. 8(a) compares this design to the 25-MHz constant-bandwidth design presented by the authors in [17]. The insertion loss in the new design has been improved by up to 0.4 dB due to the improvement in impedance matching offered by C_{ext} . This can be seen from S_{11} in Fig. 7 which is lower than -10 dB across the entire tuning range. A comparison between the measured and simulated results is shown in Fig. 8(b). The simulations assumed

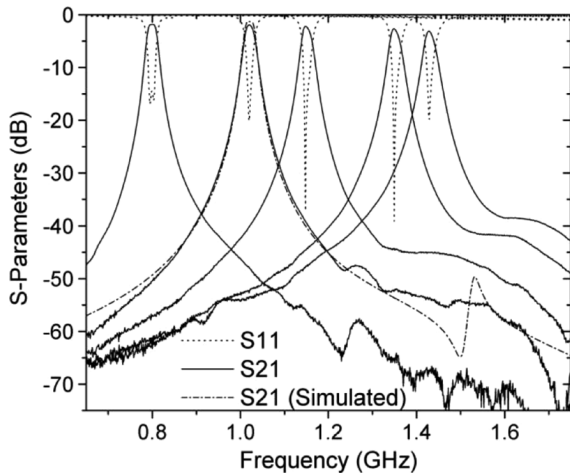


Fig. 7. Measured S parameters for the constant absolute-bandwidth filter (a simulated S_{21} response at 1.03 GHz is added for comparison).

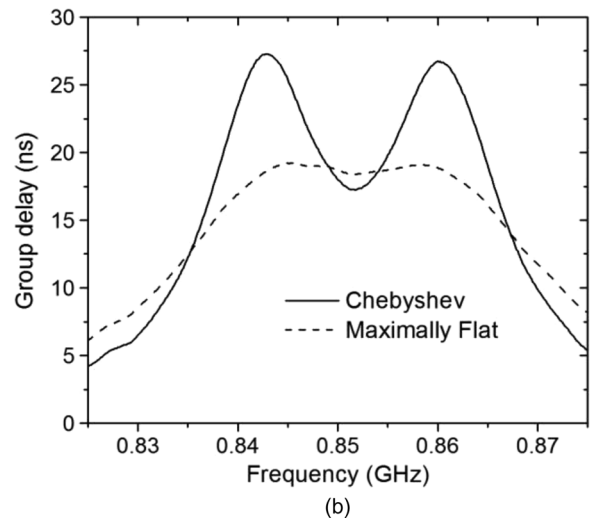
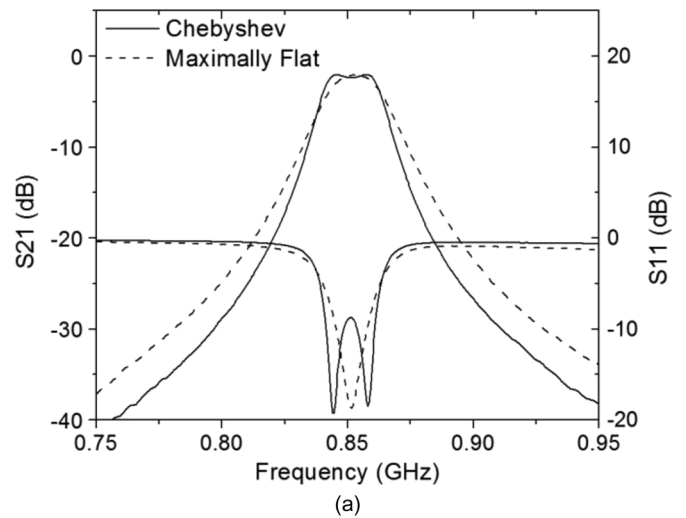


Fig. 9. Comparison of the measured filter response. (a) S parameter. (b) Group delay.

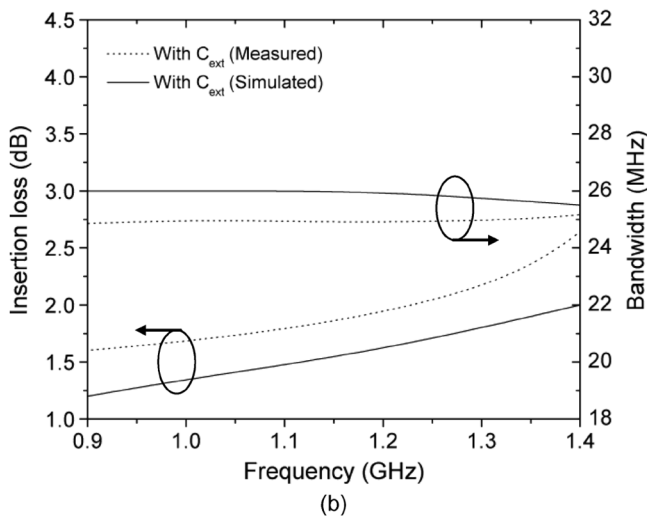
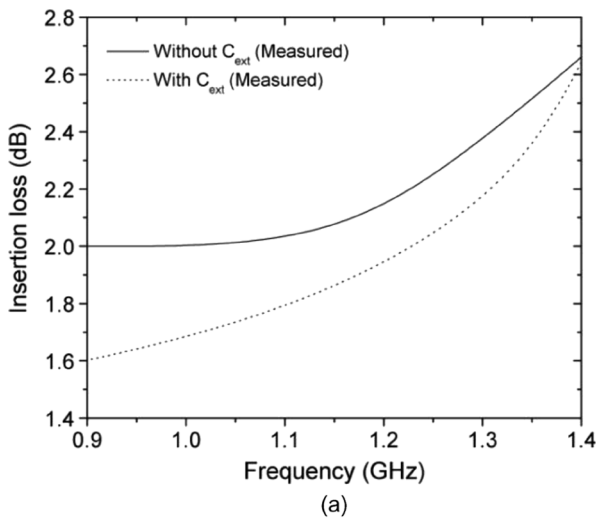


Fig. 8. (a) Measured insertion loss improvement due to C_{ext} . (b) Measured versus simulated insertion loss and bandwidth.

ideal copper conductivity and have a slightly lower insertion loss than the measured results. The varactors C_{ext} also allow control

over the out-of-band attenuation/group delay of the filter in combination with C_{var} . This is shown in Fig. 9, where the response of the filter can be both maximally flat and Chebyshev for the same bandwidth. As expected, the Chebyshev response shows a higher attenuation out of band in Fig. 9(a), while the group delay for the maximally flat response has a flatter response in the passband as seen in Fig. 9(b).

This filter is also tested for intermodulation products using the two-tone test setup shown in Fig. 10. The filter center frequency and bandwidth are monitored using two 10-dB directional couplers and an Agilent 8720ES vector network analyzer (VNA). The two input tones are separated by 0.5 MHz, and the input tones, as well as the third-order products, are measured with the filter centered at 0.8, 1, 1.2, and 1.43 GHz. The filter is set to the desired bandwidth of 25 MHz at these center frequencies, and the first- and third-order output power is measured using an Agilent E4408B spectrum analyzer. The measurements are done for three input powers for each frequency. The measured data points for the filter center frequency at 1.2 GHz are plotted in Fig. 11 versus the effective input power into the filter. The filter IIP3 is extrapolated to be 35.2 dBm and is indicated in

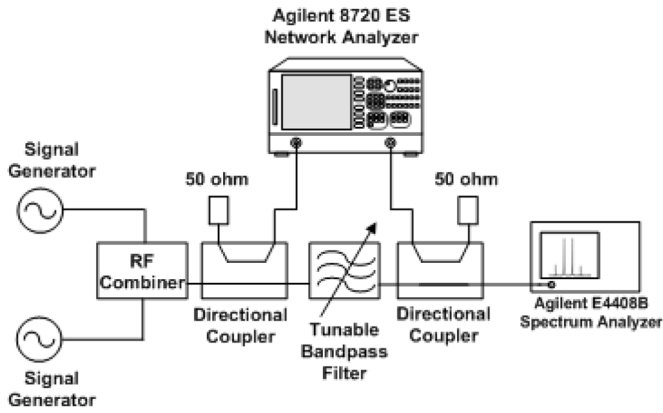


Fig. 10. Measurement setup for testing filter linearity.

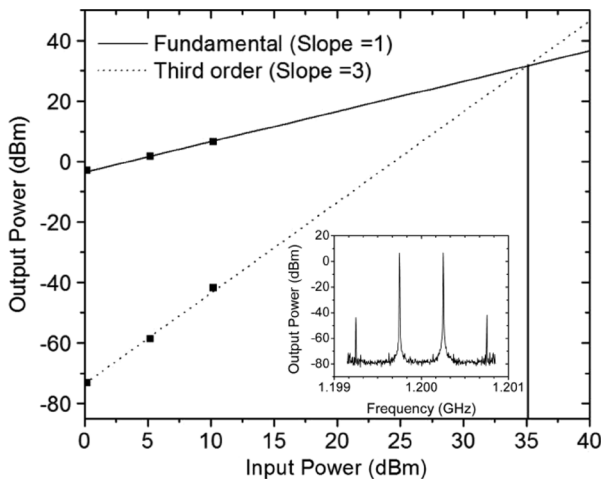


Fig. 11. IIP3 measurement results for the filter (measured values are shown as symbols). A measured output power spectrum is shown as an inset.

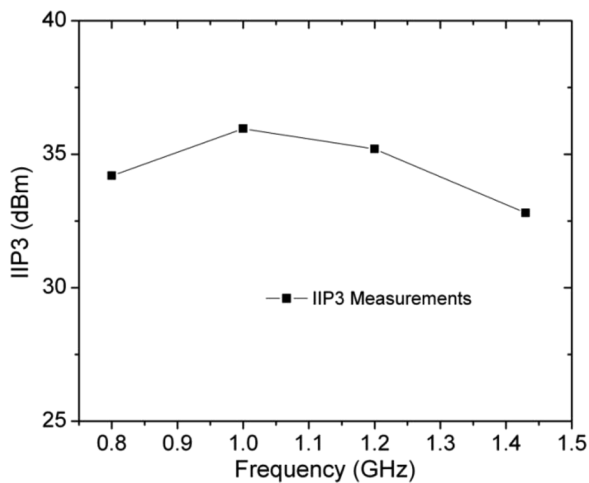


Fig. 12. Measured IIP3 results in the filter tuning range.

Fig. 11. An example of the measured output spectrum is shown as an inset in Fig. 11, where the third-order products are below -40 dBm for the highest input power. The filter IIP3 over the tuning range is plotted in Fig. 12 and has a minimum value of

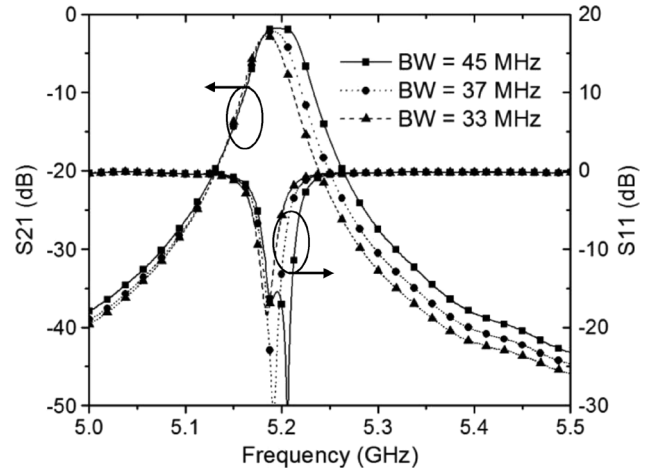


Fig. 13. Measured bandwidth control for a high- Q filter with $Q > 650$.

32.8 dBm at 1.43 GHz. This is because the bandwidth compensation using the varactors C_{var} required to maintain a 25-MHz bandwidth is maximum at 1.43 GHz, resulting in a slight increase in the third-order intermodulation products. IIP3 also reduces slightly at 0.8 GHz because the input and output coupling varactors C_{ext} are biased to a high capacitance to increase the external coupling.

B. High- Q ($Q > 500$) Filter With Bandwidth Control (3–5.6 GHz)

The design can also be extended to higher frequencies by reducing the size of the capacitive post in Fig. 6(a). For a much smaller post radius of 0.55 mm, the filter can be tuned in the range of 3–5.6 GHz with correspondingly higher Q 's in the range of 500–750 due to the increased electrical volume. To control the bandwidth variation over this tuning range, commercially available varactors MA46H120 from M/A-COM are used as C_{var} in the inter-resonator coupling mechanism. The spec sheet indicates a Q of 3000 at 50 MHz for a capacitance of 0.37 pF. This translates into an estimated Q of less than 30 at 5 GHz. In spite of this low Q , these varactors can be used for controlling the bandwidth of filters with Q as high as 750 in the 3–5.6-GHz range using the current design. This is shown in Fig. 13, where the bandwidth of a filter at 5.2 GHz is reduced from 45 to 33 MHz on increasing the varactor capacitance from about 0.2 to 0.35 pF, with the corresponding insertion loss being 1.8 and 2.8 dB, respectively. The estimated filter Q is 750 and 650, respectively, indicating a drop of less than 15% in Q for this bandwidth change of almost 27%.

The measured S parameter results for the filter when tuned from 3 to 5.6 GHz are further shown in Fig. 14. The insertion loss and bandwidth variation of the filter is shown in Fig. 15, with the insertion loss being less than 2.8 dB across the entire range. The simulations, again, assume an ideal copper conductivity and, thus, show lower loss than the measured results. The design also allows a much lower bandwidth variation than what would be due to the coupling iris alone. This is shown in Fig. 16, where the bandwidth variation over the tuning range from 3 to 5 GHz due to the coupling iris has been reduced by 54% because

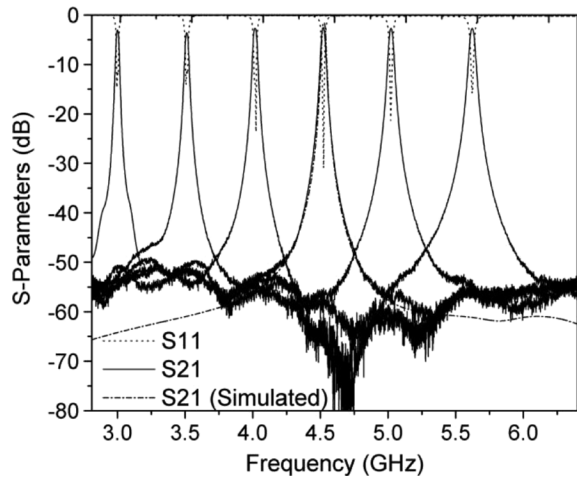


Fig. 14. Measured S parameter results for a high- Q tunable filter (a simulated S_{21} response at 4.53 GHz is added for comparison).

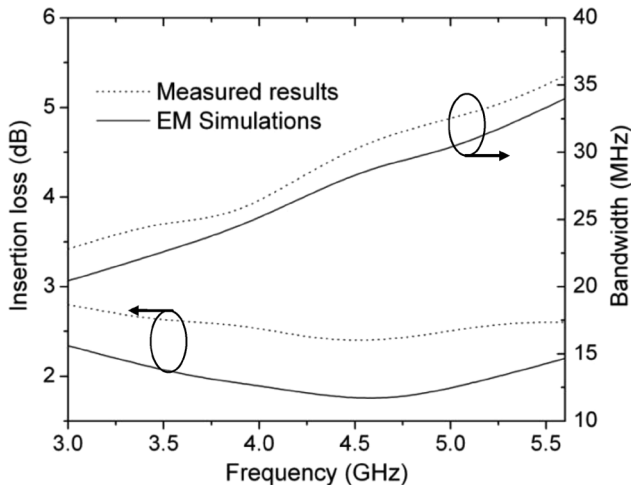


Fig. 15. Measured versus simulated performance of the high- Q filter.

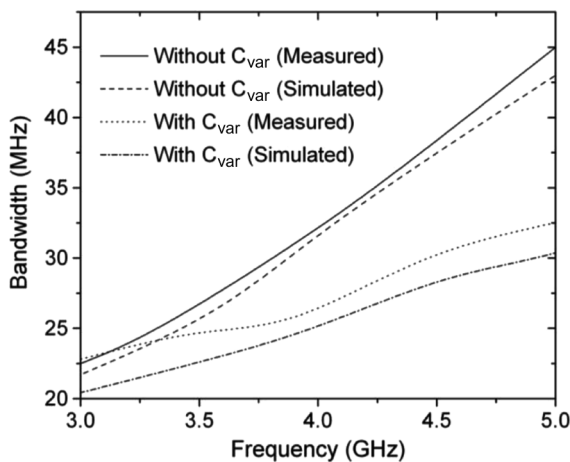


Fig. 16. Measured and simulated bandwidth variation with and without C_{var} .

of the addition of the varactors. This demonstrates the feasibility of the design concepts even for very high Q filters.

IV. CONCLUSION

A design technique to enable inter-resonator and external coupling control for high- Q narrowband filters has been presented which can utilize commercially available low- Q varactors. The design incorporates low- Q varactors so that they do not limit the overall Q of the filter. A detailed theoretical analysis is presented to explain the concepts, and an example of high- Q evanescent-mode cavity filters is used to demonstrate the practical usefulness of this design technique. A constant 25-MHz absolute-bandwidth filter is presented in the 0.8–1.43-GHz range, with less than 3.1 dB insertion loss across the entire tuning range. The design can also be extended to higher frequencies, and Q that is as high as 750 is demonstrated for a filter in the 3–5.6-GHz range. The low- Q varactors allow a bandwidth control of over 25% with less than 15% reduction in the Q of the filter. This work demonstrates high- Q reconfigurable filters with dynamic control of center frequency, bandwidth, and group delay.

REFERENCES

- [1] R. Berezdivin, R. Breinig, and R. Topp, "Next-generation wireless communications concepts and technologies," *IEEE Commun. Mag.*, vol. 40, no. 3, pp. 108–116, Mar. 2002.
- [2] A. Abbaspour-Tamijani, L. Dussopt, and G. M. Rebeiz, "Miniature and tunable filters using MEMS capacitors," *IEEE Trans. Microw. Theory Tech.*, vol. 51, no. 7, pp. 1878–1885, Jul. 2003.
- [3] W. D. Yan and R. R. Mansour, "Tunable dielectric resonator bandpass filter with embedded MEMS tuning elements," *IEEE Trans. Microw. Theory Tech.*, vol. 55, no. 1, pp. 154–160, Jan. 2007.
- [4] J. Nath, D. Ghosh, J.-P. Maria, A. I. Kingon, W. Fathelbab, P. D. Franzon, and M. B. Steer, "An electronically tunable microstrip bandpass filter using thin-film barium–strontium–titanate (BST) varactors," *IEEE Trans. Microw. Theory Tech.*, vol. 53, no. 9, pp. 2707–2712, Sep. 2005.
- [5] H. Joshi, H. H. Sigmarsson, D. Peroulis, and W. J. Chappell, "Highly loaded evanescent cavities for widely tunable high- Q filters," in *IEEE MTT-S Int. Microw. Symp. Dig.*, Jun. 3–8, 2007, pp. 2133–2136.
- [6] S.-J. Park, I. Reines, and G. M. Rebeiz, "High- Q RF-MEMS tunable evanescent-mode cavity filter," in *IEEE MTT-S Int. Microw. Symp. Dig.*, Jun. 7–12, 2009, pp. 1145–1148.
- [7] X. Liu, L. P. B. Katehi, W. J. Chappell, and D. Peroulis, "A 3.4–6.2 GHz continuously tunable electrostatic MEMS resonator with quality factor of 460–530," in *IEEE MTT-S Int. Microw. Symp. Dig.*, Jun. 7–12, 2009, pp. 1149–1152.
- [8] G. L. Matthaei, "Narrow-band, fixed-tuned, and tunable bandpass filters with zig-zag hairpin-comb resonators," *IEEE Trans. Microw. Theory Tech.*, vol. 51, no. 4, pp. 1214–1219, Apr. 2003.
- [9] I. C. Hunter and J. D. Rhodes, "Electronically tunable microwave bandpass filters," *IEEE Trans. Microw. Theory Tech.*, vol. MTT-30, no. 9, pp. 1354–1360, Sep. 1982.
- [10] B.-W. Kim and S.-W. Yun, "Varactor-tuned combline bandpass filter using step-impedance microstrip lines," *IEEE Trans. Microw. Theory Tech.*, vol. 52, no. 4, pp. 1279–1283, Apr. 2004.
- [11] S.-J. Park and G. M. Rebeiz, "Low-loss two-pole tunable filters with three different predefined bandwidth characteristics," *IEEE Trans. Microw. Theory Tech.*, vol. 56, no. 5, pp. 1137–1148, May 2008.
- [12] M. Sanchez-Renedo, R. Gomez-Garcia, J. I. Alonso, and C. Briso-Rodriguez, "Tunable combline filter with continuous control of center frequency and bandwidth," *IEEE Trans. Microw. Theory Tech.*, vol. 53, no. 1, pp. 191–199, Jan. 2005.
- [13] J. S. Sun and T. Itoh, "Dual-mode tunable filter with simple bandwidth control scheme," in *IEEE MTT-S Int. Microw. Symp. Dig.*, Jun. 7–12, 2009, pp. 497–500.
- [14] E. Fourn *et al.*, "Bandwidth and central frequency control on tunable bandpass filter by using MEMS cantilevers," in *IEEE MTT-S Int. Microw. Symp. Dig.*, Jun. 8–13, 2003, vol. 1, pp. 523–526.
- [15] R. V. Snyder, "New application of evanescent mode wave-guide to filter design," *IEEE Trans. Microw. Theory Tech.*, vol. MTT-25, no. 12, pp. 1013–1021, Dec. 1977.

- [16] G. F. Craven and C. K. Mok, "The design of evanescent mode waveguide bandpass filters for a prescribed insertion loss characteristic," *IEEE Trans. Microw. Theory Tech.*, vol. MTT-19, no. 3, pp. 295–308, Mar. 1971.
- [17] H. Joshi, H. H. Sigmarsson, S. Moon, D. Peroulis, and W. J. Chappell, "High *Q* narrowband tunable filters with controllable bandwidth," in *IEEE/MTT-S Int. Microw. Symp. Dig.*, Jun. 7–12, 2009, pp. 629–632.
- [18] G. L. Matthaei and E. M. T. Jones, *Microwave Filters, Impedance Matching Networks and Coupling Structures*. New York: McGraw-Hill, 1980.
- [19] "Infineon BB857 datasheet," Infineon Technol., Neubiberg, Germany, 2007.



Himanshu Joshi (S'06) received the B.Tech. degree in electrical engineering from the Indian Institute of Technology Kanpur, Kanpur, India, in 2004, and is currently working toward the Ph.D. degree in electrical and computer engineering at Purdue University, West Lafayette, IN.

His research interests include RF filter design, advanced packaging for microwave applications, and RF/analog circuits.



Hjalti H. Sigmarsson (S'01) received the B.S.E.C.E. degree from the University of Iceland, Reykjavik, Iceland, in 2003, the M.S.E.C.E. degree from Purdue University, West Lafayette, IN, in 2005, and is currently working toward the Ph.D. degree in electrical and computer engineering at Purdue University.

His current research focuses on tunable filter design and fabrication, advanced packaging, polymer integration on silicon, and ceramic stereolithography.

Mr. Sigmarsson is a member of the International Microelectronics and Packaging Society.



Sungwook Moon (S'06) received the B.S.E.E. and M.S.E.E. degrees from Kwangwoon University, Seoul, Korea, in 1995 and 1997, respectively, and is currently working toward the Ph.D. degree in electrical and computer engineering at Purdue University, West Lafayette, IN.

From 1997 to 2001, he was with the Taihan Electric Wire Company Ltd., where he was involved in the development of high-speed transceivers for 2.5-G optical transmission. From 2001 to 2006, he was with LG Cable Ltd., where he was involved with a project

on an optical thin-film filter packaging and low-cost hybrid optical transceiver based on passive alignment. His current research focuses on RF characterizations of anisotropic conductive adhesives, vertical RF interconnects, and tunable evanescent-mode cavity resonators.



Dimitrios Peroulis (S'99–M'04) received the Diploma degree in electrical and computer engineering from the National Technical University of Athens, Athens, Greece, in 1998, and the M.S.E.E. and Ph.D. degrees in electrical engineering from The University of Michigan at Ann Arbor, in 1999 and 2003, respectively.

He is currently an Associate Professor with the Schools of Electrical and Computer Engineering and Mechanical Engineering, Purdue University, West Lafayette, IN. His group is currently part of the IMPACT Center funded by the Defense Advanced Research Projects Agency (DARPA) and the PRISM Center funded by the National Nuclear Security Administration that are focused on MEMS failure mechanisms and reliability. He also leads unique research efforts in high-*Q* widely tunable reconfigurable MEMS filters, real-time reconfigurable matching networks for pulse-based systems, and harsh-environment sensors for health monitoring of aircraft engines and structures. His research is focused on multifunctional communication systems and sensors.

Dr. Peroulis was the recipient of the National Science Foundation (NSF) CAREER Award and the Semiconductor Research Corporation IC Design Challenge 1st Place Award in Phases I and II in 2008. He was also the recipient of six teaching awards from Purdue University, including the Teaching for Tomorrow Award (2006) and the Potter Award (2008). His students have received Student Paper Awards in several IEEE Microwave Theory and Techniques Society (IEEE MTT-S) International Microwave Symposia.



William J. Chappell (S'98–M'02) received the B.S.E.E., M.S.E.E., and Ph.D. degrees from The University of Michigan at Ann Arbor, in 1998, 2000, and 2002, respectively.

He is currently an Assistant Professor with the School of Electrical and Computer Engineering, Purdue University, West Lafayette, IN, where he is also a Member of the Birck Nanotechnology Center and the Center for Wireless Systems and Applications. His research focus is on advanced applications of RF and microwave components. He

has been involved with numerous Defense Advanced Research Projects Agency (DARPA) projects involved in advanced packaging and material processing for microwave applications. His research sponsors include HSARPA, ONR, NSF, the state of Indiana, CERDEC, and ARO, as well as industry sponsors. His research group uses electromagnetic analysis, unique processing of materials, and advanced design to create novel microwave components. His specific research interests are the application of very high-quality and tunable components utilizing multilayer packages. In addition, he is involved with high-power RF systems, packages, and applications.

Dr. Chappell was the IEEE Microwave Theory and Techniques Society (IEEE MTT-S) Administrative Committee (AdCom) secretary for 2009 and was elected to the IEEE MTT-S AdCom for 2010–2012.